Proceedings of the Reactor Physics Asia 2015 (RPHA15) Conference
Jeju, Korea, Sept. 16-18, 2015

Implementation of the First Collision Source Method for a Volume Source in a Three-Dimensional, Unstructured Tetrahedral Mesh, Discrete-Ordinates Code

Jong Woon KIM* and Young-Ouk LEE
Korea Atomic Energy Research Institute, 989 Daeduck-daero, Yuseong-gu, Daejeon 305-353, Korea
*Corresponding author: jwkim@kaeri.re.kr

1. Introduction

As with any discrete-ordinates code, ray-effect is an inherent problem, especially for shielding type problems with optically thin regions and localized (point) sources. Although increasing the quadrature order can mitigate the ray-effect, doing so is often computationally prohibitive.

To mitigate the ray-effect, many discrete-ordinates codes use the first collision source (FCS) method. Such method is characterized by a decomposition of the flux into its uncollided and collided components.

The uncollided flux is calculated analytically, and the collided flux is calculated using the discrete-ordinates method.

In this paper, the implementation of the first collision source method for a volume source in a three-dimensional, unstructured tetrahedral mesh, discrete-ordinates code is presented, and the results are compared with that of MCNP6.

2. Method and Results

2.1 Derivation of the Governing Equation

The first collision source method for the point source is already implemented in our program [1-3]. In this paper, we like to apply the first collision source method on a volume source.

This is not new. FNSUNCL3 [4] was developed as an FCS calculation code for TORT.

Our program is different from others that our program uses an unstructured tetrahedral mesh, and thus can be applied to solve the radiation transport in a complicated geometry.

We modify the volume source to the several pseudo-point sources as Fig. 1.

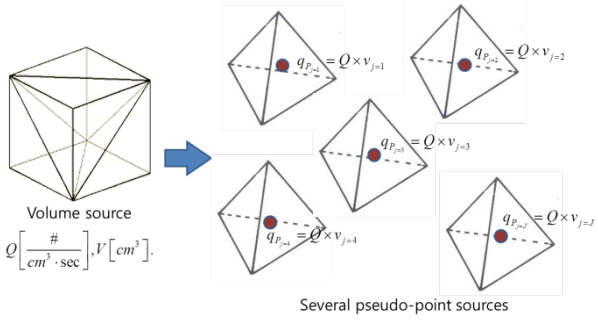

Fig. 1. Convert volume source to the several pseudo-point sources.

The source zone has source strength Q [#/cm^3·sec], total volume V [cm^3], and consists of J tetrahedral elements.

We can convert the volume source to the several pseudo- point sources, q_{p_j} [#/ sec] , as

$$q_{p_j} = Q \times v_j,$$
$$V = \sum_{j=1}^{J} v_j, \tag{1}$$

where v_j is the volume of tetrahedral element which belongs to the source zone.

Then, apply the first collision source method on the several pseudo-point sources.

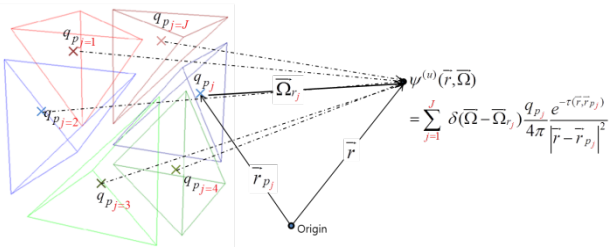

Fig. 2. The concept of this method.

The one-group transport equation with vacuum boundaries and isotropic point sources at $\vec{r}_{p_j}$ is

$$\vec{\Omega}\cdot\nabla\psi(\vec{r},\vec{\Omega}) + \sigma_t(\vec{r})\psi(\vec{r},\vec{\Omega}) = \sum_{\ell=0}^{L}\sigma_{s,\ell}(\vec{r})\sum_{m=-\ell}^{\ell}Y_{\ell,m}^{*}(\vec{\Omega})\Phi_\ell^m(\vec{r}) + \sum_{j=1}^{J}\frac{q_{p_j}}{4\pi}\delta(\vec{r}-\vec{r}_{p_j}), \tag{2}$$

where J is the total number of tetrahedral elements belonging to the volume source zone, and the moments of the angular flux is

$$\Phi_\ell^m(\vec{r}) = \int d\vec{\Omega}\, Y_{\ell,m}(\vec{\Omega})\psi(\vec{r},\vec{\Omega}). \tag{3}$$

Decompose the angular flux into two components as

$$\psi(\vec{r},\vec{\Omega}) = \psi^{(u)}(\vec{r},\vec{\Omega}) + \psi^{(c)}(\vec{r},\vec{\Omega}), \tag{4}$$

where $\psi^{(u)}(\vec{r},\vec{\Omega})$ is the uncollided angular flux and $\psi^{(c)}(\vec{r},\vec{\Omega})$ is the collided angular flux.

Rewriting Eq. (2) with Eq. (4), we have two equations

$$\vec{\Omega}\cdot\nabla\psi^{(u)}(\vec{r},\vec{\Omega})+\sigma_t(\vec{r})\psi^{(u)}(\vec{r},\vec{\Omega})=\sum_{j=1}^{J}\frac{q_{p_j}}{4\pi}\delta(\vec{r}-\vec{r}_{p_j}), \tag{5a}$$

$$\vec{\Omega}\cdot\nabla\psi^{(c)}(\vec{r},\vec{\Omega})+\sigma_t(\vec{r})\psi^{(c)}(\vec{r},\vec{\Omega}) =\sum_{\ell=0}^{L}\sigma_{s,\ell}(\vec{r})\sum_{m=-\ell}^{\ell}Y_{\ell,m}^{*}(\vec{\Omega})\Phi_{\ell}^{m,(c)}(\vec{r})+q_s^{(u)}(\vec{r}). \tag{5b}$$

Equation (5a) can be solved analytically for an uncollided angular flux, and $r_{\min}$ is introduced to prevent it from dividing by zero or a very small distance.

$$\psi^{(u)}(\vec{r},\vec{\Omega})=\begin{cases}\sum_{j=1}^{J}\delta(\vec{\Omega}-\vec{\Omega}_{r_j})\frac{q_{p_j}}{4\pi}\frac{e^{-\tau(\vec{r},\vec{r}_{p_j})}}{\left|\vec{r}-\vec{r}_{p_j}\right|^2}, & \left|\vec{r}-\vec{r}_{p_j}\right|\geq r_{\min},\\ \sum_{j=1}^{J}\delta(\vec{\Omega}-\vec{\Omega}_{r_j})\frac{q_{p_j}}{4\pi}\frac{1}{r_{\min}^2}, & \left|\vec{r}-\vec{r}_{p_j}\right|<r_{\min}.\end{cases} \tag{6}$$

The first collision source, $q_s^{(u)}(\vec{r})$, is defined as

$$q_s^{(u)}(\vec{r})=\sum_{\ell=0}^{L}\sigma_{s,\ell}(\vec{r})\sum_{m=-\ell}^{\ell}Y_{\ell,m}^{*}(\vec{\Omega})\Phi_{\ell}^{m,(u)}(\vec{r}). \tag{7}$$

The spherical harmonic moments of the uncollided angular flux, $\Phi_{\ell}^{m,(u)}(\vec{r})$, is calculated as

$$\Phi_{\ell}^{m,(u)}(\vec{r})=\int d\vec{\Omega}\,Y_{\ell,m}(\vec{\Omega})\psi^{(u)}(\vec{r},\vec{\Omega}) =\begin{cases}\sum_{j=1}^{J}Y_{\ell,m}(\vec{\Omega}_{r_j})\frac{q_{p_j}}{4\pi}\frac{e^{-\tau(\vec{r},\vec{r}_{p_j})}}{\left|\vec{r}-\vec{r}_{p_j}\right|^2}, & \left|\vec{r}-\vec{r}_{p_j}\right|\geq r_{\min},\\ \sum_{j=1}^{J}Y_{\ell,m}(\vec{\Omega}_{r_j})\frac{q_{p_j}}{4\pi}\frac{1}{r_{\min}^2}, & \left|\vec{r}-\vec{r}_{p_j}\right|<r_{\min},\end{cases} \tag{8}$$

where $\tau(\vec{r},\vec{r}_{p_j})$ is the optical distance between $\vec{r}$ and $\vec{r}_{p_j}$.

The optical distance from the pseudo-point sources to each position, where the uncollided flux is calculated, is calculated with

$$\tau(\vec{r},\vec{r}_{p_j})=\sum_{i=1}^{N}r_i\sigma_{t,i}. \tag{9}$$

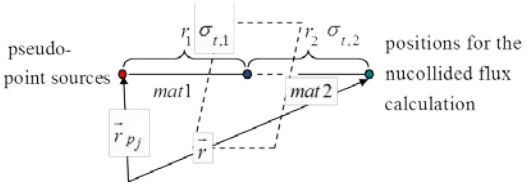

Fig. 3. The optical distance at the material interface.

2.2 Tests and Results

For verification, the Test Problem is configured as shown in Fig. 4. The volume source (10×10×10 cm^3) is located at the corner of a 100×100×100 cm^3 cube.

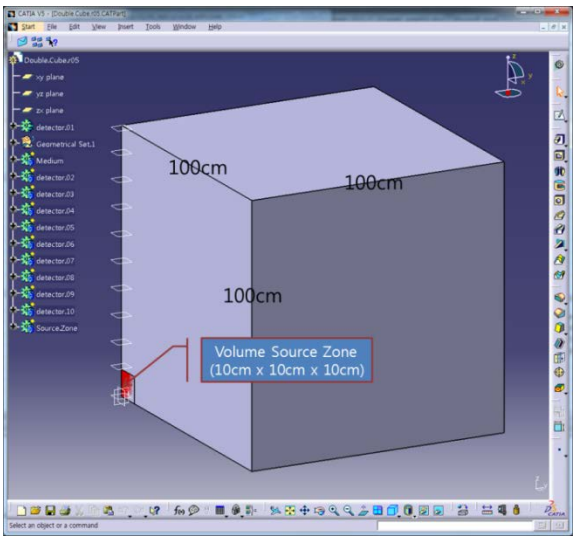

Fig. 4. The modeling of the Test Problem.

To compare our results with that of the reference calculation (MCNP6), we set ten detector volumes along the diagonal line, as shown in Fig. 5. The size of the detector volume is 0.2 mm × 0.2 mm × 0.2 mm.

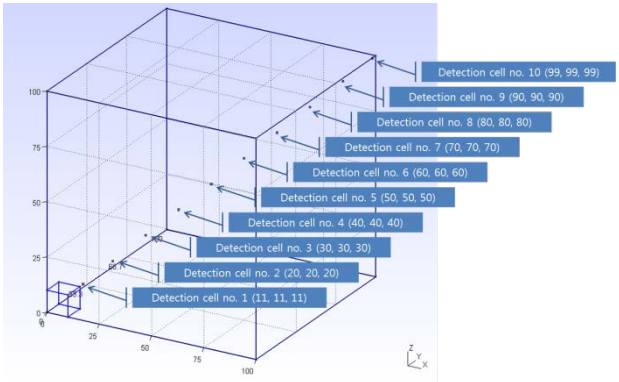

Fig. 5. The locations of ten detectors in the Test Problem (dx=dy=dz=2mm).

The computational mesh is generated by Gmsh [6] and is shown in Fig. 6.

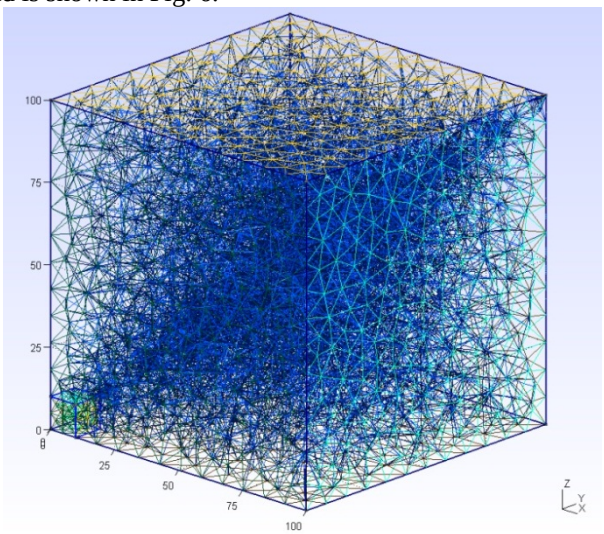

Fig. 6. The computational mesh (generated by Gmsh, 36,175 unstructured tetrahedrons).

The parameters for the numerical tests are listed in Table I. The reference fluxes on the ten detector volumes are calculated with MCNP6 [5].

Table I. Parameters for the Test Problem

Source	
1 particle/sec in volume source zone	
Geometry	
Volume of source zone	1,000 cm^3
Volume of other zone	999,000 cm^3
MCNP6	
Continuous energy, f4 tally, 1 particle/sec in volume source zone with 1st group of LANL-30 group structure	
S_N	
No. of tetrahedron in source zone	130
No. of tetrahedron in other zone	36,045
Volume source	1.0e-3 #/cm^3·sec in 1st group of LANL-30
Group structure	LANL-30
S_N order	16
Error criterion	1.0e-4
Material	
Density	0.001293 g/cm^3
Isotopes	N14 / 7.757e-01
/weight fraction	N15 / 2.850e-03
	O16 / 2.209e-01
	O17 / 5.314e-04

Two options are used in the FCS method and shown in Fig. 7.

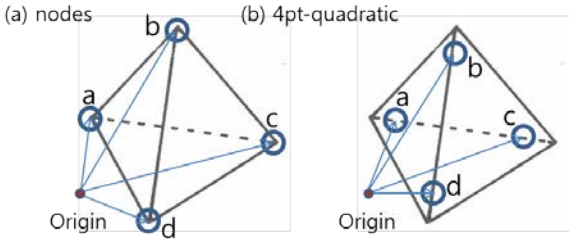

Fig. 7. Two options of FCS method; (a) nodes, (b) 4pt-quadratic.

For the node base scheme, the uncollided flux is calculated on the node positions, so that uncollided flux is continuous on the boundaries of elements. As we can see in the Fig. 8, if flux is changing drastically within the element, this scheme may overestimate the real flux distribution.

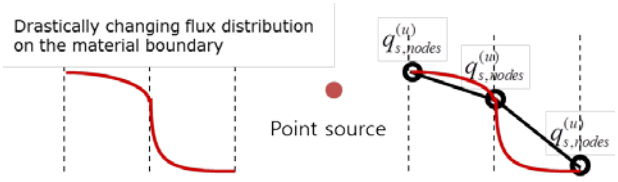

Fig. 8. Node base scheme (continuous scheme).

For the 4pt-quadratic scheme, the uncollided fluxes are calculated on the four points listed in the Table II and use them as uncollided fluxes on the four vertexes. This scheme allows discontinuity at the boundary of the tetrahedral elements like Fig. 9 [3].

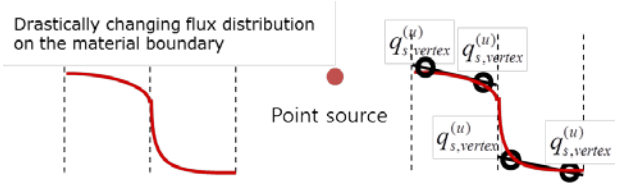

Fig. 9. 4-pt quadratic scheme (discontinuous scheme).

Table II. Positions where uncollided fluxes are calculated with 4pt-quadratic scheme [7]

Figure	Error	Points	Tetrahedral Coordinates	Weights
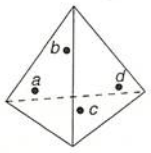	$R=O(h^3)$	*a*	$\alpha, \beta, \beta, \beta$	1/4
		b	$\beta, \alpha, \beta, \beta$	1/4
		c	$\beta, \beta, \alpha, \beta$	1/4
		d	$\beta, \beta, \beta, \alpha$	1/4
			α=0.58541020	
			β=0.13819660	

The calculated results are compared with that of MCNP6, and are listed in Table III.

Compared to the MCNP6 results, the volume source only shows large differences. The reason for this can be explained through the total flux distribution shown in Fig. 10. Even when we use the S_{16} quadrature, the ray-effect is still dominant.

However, for the case of the first collision source method on the volume, the averaged flux over the detector zones gives much closer results than that with the volume source only with a maximum error of -4.7%.

Table III. The flux averaged over detector zones

x/ y/ z/ [cm]	MCNP6	Volume source	First collision source method on volume	
			nodes	4pt-quadratic
11	8.34215E-04 [0.0357]†	8.67368E-04 (3.974)§	8.36516E-04 (0.276)§	8.36532E-04 (0.278)§
20	1.25256E-04 [0.0583]	1.17027E-04 (-6.570)	1.19358E-04 (-4.709)	1.19354E-04 (-4.712)
30	4.23126E-05 [0.0046]	1.49161E-05 (-64.748)	4.26023E-05 (0.685)	4.25987E-05 (0.676)
40	2.15822E-05 [0.0064]	8.30670E-06 (-61.511)	2.16823E-05 (0.464)	2.16808E-05 (0.457)
50	1.31374E-05 [0.0082]	3.97819E-06 (-69.719)	1.30999E-05 (-0.285)	1.30988E-05 (-0.294)
60	8.70456E-06 [0.0101]	1.53403E-06 (-82.377)	8.75999E-06 (0.637)	8.75938E-06 (0.630)
70	6.28582E-06 [0.0119]	2.18502E-07 (-96.524)	6.26456E-06 (-0.338)	6.26425E-06 (-0.343)
80	4.51771E-06 [0.0140]	-1.89240E-07 (-104.189)	4.69997E-06 (4.034)	4.69979E-06 (4.030)
90	3.62394E-06 [0.0156]	-1.80894E-07 (-104.992)	3.65533E-06 (0.866)	3.65521E-06 (0.863)
99	2.86806E-06 [0.0176]	-1.96775E-07 (-106.861)	2.98486E-06 (4.072)	2.98478E-06 (4.070)

† relative error of MCNP6
§ [(Result-MCNP6)/MCNP6]×100

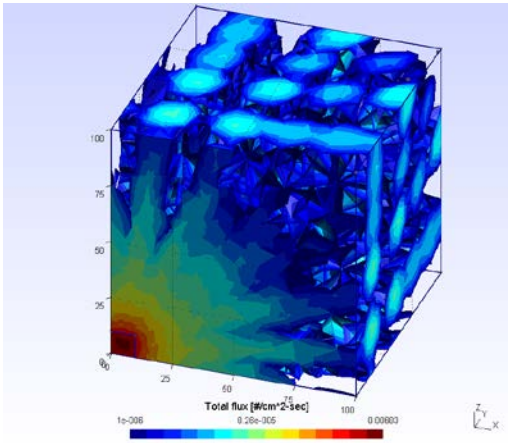

Fig. 10. Total flux distribution with the volume source only (S_{16}).

Two total flux distributions with nodes and a 4pt-quadratic [3] are shown in Figs. 11 and 12, and the ray effect cannot be observed.

In the case of the nodes, the fluxes are continuous between neighbor nodes such that the flux distribution is very smooth.

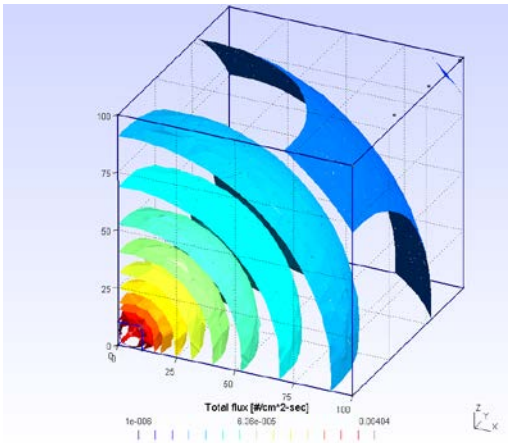

Fig. 11. Total flux distribution with the first collision source method on the volume source (nodes).

However, in the case of a 4pt-quadratic, points, where uncollided fluxes are calculated, are slightly off from the four vertices such that the flux distribution in Fig. 12 looks like tiles on the isosurfaces. The two different features (continuous and discontinuous) can be seen in the total flux distributions in Figs. 11 and 12.

The discontinuous method gives better results than that with the continuous method when the fluxes are changed rapidly by passing through the shielding material.

However, the two results are similar because the Test Problem consists of only air (no shielding material to reduce flux drastically).

The sensitivity study of this method with a different tetrahedral element size in the volume source zone has not been performed yet. However, we can presume that the smaller sized elements in the volume source zone may give better results than that with bigger sized elements.

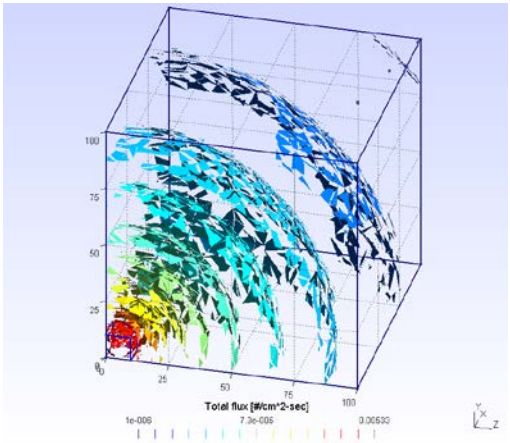

Fig. 12. Total flux distribution with the first collision source method on the volume source (4pt-quadratic).

3. Conclusions

In this paper, we present the results of the FCS method on the volume source by modifying the volume source to the pseudo-point sources. We confirmed that the FCS method on the volume source was successfully implemented in our program.

A modification to add or enhance the functions of our program will be performed.

References

1. Kim J W, Hong S G, and Lee Y, “Implementation of the First Collision Source Method in a Three-Dimensional, Unstructured Tetrahedral Mesh, Discrete-Ordinates Code,” Transaction of the Korean Nuclear Society Autumn Meeting, Gyeongju, Korea (2009).
2. Kim J W, Hong S G, and Lee Y, “A Comparison of Energy Spectra Computed with Continuous and Discontinuous Schemes for Uncollided Flux Calculation on the First Collision Source Method,” Transaction of the Korean Association for Radiation Protection Spring Meeting, Mokpo, Korea (2013).
3. Kim J W and Lee Y, “A Comparison of Dose Distributions Computed with Three Schemes for Uncollided Flux Calculation on the First Collision Source Method,” Transaction of the Korean Nuclear Society Spring Meeting, Gwangju, Korea (2013).
4. Kosako K and Konno C, “FNSUNCL3: First Collision Source Code for TORT,” Journal of Nuclear Science and Technology, 37:sup1, 475-478 (2014).
5. MCNP6TM User’s Manual Version 1.0, LA-CP-13-00634, Rev. 0. (2013).
6. Geuzaine C and Remacle J -F, “Gmsh: a three-dimensional finite element mesh generator with built-in pre- and post-processing facilities,” Int. J. Numer. Meth. Eng. 79 (11), 1309-1331 (2009).
7. Zienkiewicz O C, Taylor R L, and Zhu J Z, The Finite Element Method: Its Basic and Fundamentals, Sixth edition, ELSEVIER, pp.164-167 (2005).